An approach to sulfate geoengineering with surface emissions of carbonyl sulfide

Ilaria Quaglia[1], Daniele Visioni[2], Giovanni Pitari[1], and Ben Kravitz[3,4]

[1]Department of Physical and Chemical Sciences, Università dell'Aquila, 67100 L'Aquila, Italy
[2]Sibley School for Mechanical and Aerospace Engineering, Cornell University, Ithaca, NY 14853, USA
[3]Department of Earth and Atmospheric Science, Indiana University, Bloomington, IN, USA
[4]Atmospheric Sciences and Global Change Division, Pacific Northwest National Laboratory, Richland, WA, USA

Correspondence: Ilaria Quaglia (ilaria.quaglia@aquila.infn.it)

Abstract. Sulfate geoengineering (SG) methods based on lower stratospheric tropical injection of sulfur dioxide (SO_2) have been widely discussed in recent years, focusing on the direct and indirect effects they would have on the climate system. Here a potential alternative method is discussed, where sulfur emissions are located at the surface or in the troposphere in the form of carbonyl sulfide (COS) gas. Two time-dependent chemistry-climate model experiments are designed from year 2021 to 2055, assuming a 40 Tg-S/yr artificial global flux of COS, geographically distributed following the present day anthropogenic COS surface emissions (SG-COS-SRF), or a 6 Tg-S/yr injection of COS in the tropical upper troposphere (SG-COS-TTL). The budget of COS and sulfur species is discussed, as well as the effects of both SG-COS strategies on the stratospheric sulfate aerosol optical depth ($\sim \Delta\tau$=0.080 in years 2046-2055), aerosol effective radius (0.46 μm), surface SO_x deposition (+8.9 % for SG-COS-SRF, +3.3 % for SG-COS-TTL) and tropopause radiative forcing (RF) ($\sim$ -1.5 W/m^2 in All Sky conditions in both SG-COS experiments). Indirect effects on ozone, methane and stratospheric water vapor are also considered, along with the COS direct contribution. According to our model results, the resulting net RF is -1.3 W/m^2 for SC-COS-SRF and -1.5 W/m^2 for SG-COS-TTL, and it is comparable to the corresponding RF of -1.7 W/m^2 obtained with a sustained injection of 4 Tg-S/yr in the tropical lower stratosphere in the form of SO_2 (SG-SO2, able to produce a comparable increase of the sulfate aerosol optical depth). Significant changes of the stratospheric ozone response are found in both SG-COS experiments with respect to SG-SO2 ($\sim$5 DU versus +1.4 DU, globally). According to the model results, the resulting UVB perturbation at the surface accounts for -4.3% as a global-annual average (versus –2.4% in the SG-SO2 case), with a springtime Antarctic decrease of -2.7% (versus a +5.8% increase in the SG-SO2 experiment). Overall, we find that an increase in COS emissions may be feasible, and produce a more latitudinally-uniform forcing without the need for the deployment of stratospheric aircrafts.

1 Introduction

Reducing part of the incoming solar radiation (known as Solar Radiation Modification, SRM) has been proposed as a strategy for reducing surface temperatures and thus mitigating some of the worst side-effects of the greenhouse gases-induced global warming (Budyko, 1977; Institute of Medicine and National Academy of Sciences and National Academy of Engineering, 1992; Crutzen, 2006). Various methods have been proposed to achieve this: the injection of sulfate precursors into the lower

stratosphere to obtain a cloud of aerosols capable of reflective a portion of the incoming sunlight has been, by far, the most studied due to the observation of a similar cooling effect produced by explosive volcanic eruptions in the past (Robock, 2000). While preliminary estimates for the cost of an eventual deployment already exist (Smith and Wagner, 2018), from an engineering perspective there are no known technologies readily available to carry SO_2 or any other precursors considered up to now from the ground up to the lower stratosphere in the quantities needed to obtain a noticeable effect on the surface climate (Lockley et al., 2020). Since any proposed compound would quickly react to form sulfate aerosols, they would need to be carried sealed to the desired altitude, and then released, to ensure a high enough lifetime compared to that of the same aerosols in the troposphere (Lamarque et al., 2013).

We explore here a different approach to increasing the aerosol optical depth in the stratosphere, that makes use of emissions of a gaseous precursor of sulfate aerosols: carbonyl sulfide (COS). COS has a long atmospheric lifetime (4 to 6 years; Khalil and Rasmussen, 1984; Ulshofer et al., 1996) due to its very low reactivity in the troposphere. Because of this, it is also uniformly mixed in the atmosphere, with an average concentration of 0.5 ppbv, and therefore it easily reaches the stratosphere: in quiescent volcanic conditions, COS is the main contributor of sulfate aerosols in the Junge layer (Brühl et al., 2012), where after photodissociation by ultraviolet light and oxidation processes, it is turned into SO_2 and subsequently oxidized into sulfuric acid, forming sulfate aerosols (Crutzen, 1976). It is naturally produced by various biological processes and environments, such as saline ecosystems, rainwaters (Mu et al., 2004) and biomass burning. Furthermore, it is also produced in various industrial processes (Lee and Brimblecombe, 2016) after CS_2 is oxidized. Its chemical life is very long (35 years; Brühl et al., 2012) and thus its main sink is the uptake from oxic soils (Kuhn and Kesselmeier, 2000; Steinbacher et al., 2004) and vegetation (Sandoval-Soto et al., 2005). In the concentrations found in the atmosphere, it is not a toxic gas for humans: negative effects have not been found even at around 50 ppm, which is 100,000 times more than the background mixing ratio, and for long exposure times in mice and rabbits (Svoronos and Bruno, 2002). Higher concentrations than that can, however, be harmful (Bartholomaeus and Haritos, 2006). Not much is known however about the response of ecosystems in the presence of high concentrations of COS: Stimler et al. (2010) showed that high levels of COS enhance the stomatal conductance of some plants, which might in turn have other unforeseen effects; further, Conrad and Meuser (2000) proposed that high COS concentrations may interact with soils and possibly change soil pH. For the reasons listed above, Crutzen (2006) discarded the idea of using surface emissions of COS to increase the stratospheric aerosol burden.

In this work, we use the University of L'Aquila-Climate-Chemistry Model (ULAQ-CCM) to perform simulations to verify if the increase in surface emissions of COS would be a viable form of sulfate geoengineering, by obtaining a stratospheric aerosol optical depth (AOD) similar to that obtained with the injection of 8 Tg-SO_2 in the stratosphere. We also perform simulations where the release of COS is localized in the tropical upper troposphere. This allows us to investigate whether the increase in surface concentrations of COS can be avoided while at the same time circumventing the need to reach altitude currently unattainable with modern aircrafts (Smith et al., 2020). Together with assessing the resulting aerosol cloud, we also explore the eventual side-effects on key chemical components in the atmosphere, in order to determine how the side effects from COS-induced Sulfate Geoengineering compare with those from SO_2-induced Sulfate Geoengineering. For the latter, there is ample literature assessing its effect on stratospheric ozone (Tilmes et al., 2008; Pitari et al., 2014; Xia et al., 2017a; Vattioni et al.,

2019): the increase in surface area density, stratospheric heating and dynamical effect all play a part in determining the overall

60 changes (Tilmes et al., 2018b; Richter et al., 2017) to the ozone column that, in turn, determine the changes in surface UV (Visioni et al., 2017b; Madronich et al., 2018) that would be important when considering adverse health effects (Eastham et al., 2018).

2 Model description and setup of numerical experiments
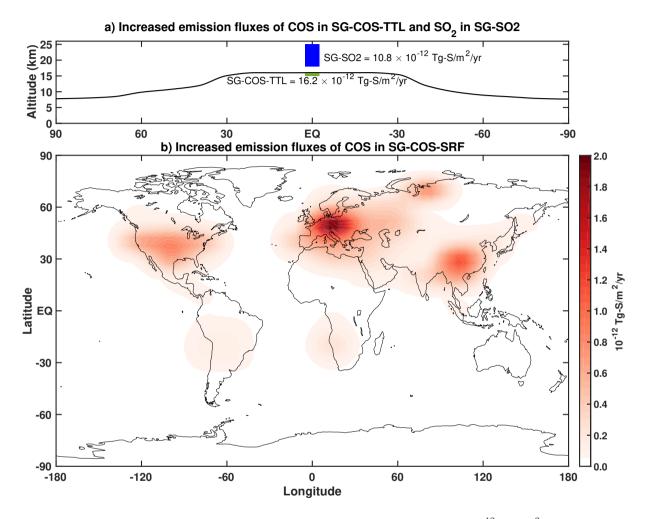
The simulations presented in this paper have been carried out with the University of L'Aquila Climate-Chemistry Model

65 (ULAQ-CCM), a CCM robustly tested and used before in evaluation of the radiative, chemical and dynamical effects of stratospheric and tropospheric aerosols (Pitari et al., 2002; Eyring et al., 2006; Morgenstern et al., 2010). It has also been used for various sulfate geoengineering simulations (Pitari et al., 2014; Visioni et al., 2018a, b) and, as part of the Climate-Chemistry Model Intercomparison project (Morgenstern et al., 2018), where it has been extensively validated with other CCMs. The high vertical resolution (127 levels) allows for a proper representation of large-scale transport of gas and aerosol species

70 in the troposphere (Orbe et al., 2018) and in the stratosphere (Visioni et al., 2017b; Eichinger et al., 2019), and the detailed chemistry, including heterogeneous chemical reactions on sulfuric acid aerosols, polar stratospheric cloud particles, upper tropospheric ice and liquid water cloud particles allows for a full assessment of the effects of the increased sulfate burden on the atmospheric composition. ULAQ-CCM simulated COS also compares reasonably well with available measurements of seasonal COS concentrations (see Fig. S1) from Kuai et al. (2015), with an average annual error of 6.5%, albeit with peaks in

75 some areas and months of up to 30%.

In addition to a reference historical model experiment (1960-2015), we performed four sets of simulations: a baseline unperturbed (BG) case and three geoengineering experiments (SG-COS-SRF, SG-COS-TRP and SG-SO2), all run between the years 2021-2055, with analyses focusing on the 2046-2055 decade; all experiments take place under the Representative Concentration Pathway 6.0 (RCP; Meinshausen et al., 2011) emissions.

80 The first geoengineering experiment, SG-COS-SRF, tries to produce a significant stratospheric aerosol burden by enhancing current anthropogenic emission of COS (0.12 Tg-S/yr, see table S1) by 40 Tg-S/yr. These emissions are located at the ground, in the main regions of anthropogenic COS surface emissions (see Fig. 1). The second experiment, SG-COS-TTL, tries to replicate the same stratospheric aerosol burden as SG-COS-SRF by injecting 6 Tg-S/yr of COS directly below the tropopause, at 16 km of altitude and at the equator. In the following text, whenever we are referring to results pertaining to both COS

85 experiments, we will use the term SG-COS. Finally, the experiment SG-SO2, similarly to previous experiments discussed in the literature (Kravitz et al. (2011) in the G4 experiment), consists of the injection of 4 Tg-S/yr in the form of SO_2 at the equator, between 18 and 25 km of altitude.

For the geoengineering experiments, ULAQ-CCM is driven by time-dependent sea surface temperatures (SSTs) from the Community Climate System Model – Community Atmosphere Model version 4 (CCSM-CAM4; Neale et al., 2013), an

90 atmosphere-ocean coupled model that ran similar geoengineering experiments as in SG-SO2 (described by Tilmes et al., 2015): this allows for the inclusion of the cooling produced by geoengineering on the surface to the assessment of the dynamical and

Figure 1. a) Vertical and latitudinal distribution of COS emissions per year and unit of surface area (10^{-12} Tg-S/m^2/yr) in the SG-COS-TTL experiment (green box) and SO$_2$ emission fluxes in the same unit in SG-SO2 (blue box). The quantities are distributed in a single vertical level for SG-COS-TTL, and in 12 vertical levels for SG-SO2. b) Geographical distribution of COS emission fluxes per year and unit of surface area (10^{-12} Tg-S/m^2/yr) in the SG-COS-SRF experiment. The annual upward flux is averaged over the period 2046-2055.

chemical effect as simulated by ULAQ-CCM. To include the important radiative effects produced by other atmospheric components (mainly, geoengineering-driven changes in greenhouse gases concentration and in ice clouds; Visioni et al., 2017b, 2018a) the radiative module of ULAQ-CCM calculates at each time-step the surface temperature perturbation produced by the radiative flux changes induced by these components and includes them in the CCSM-CAM4 SSTs. This approach has been further explained and validated by Visioni et al. (2018a). While the prescribed SST setup has been shown to correctly capture dynamical changes produced by SRM (Visioni et al., 2017b), it clearly does not capture potential feedbacks that may be relevant for surface climate, such as those produced by the different latitudinal distribution of the aerosol optical depth that we will show later on. These differences may also in turn feed back onto changes in COS lifetime through precipitation changes (Whelan et al., 2016) which we can't consider here. We will therefore limit ourselves to analyzing changes in atmospheric composition and dynamics, and how those contribute to the overall radiative forcing from the aerosols. Future experiments with a more comprehensive Earth-system model will be necessary to determine the full extent of the climatic response.

3 Results
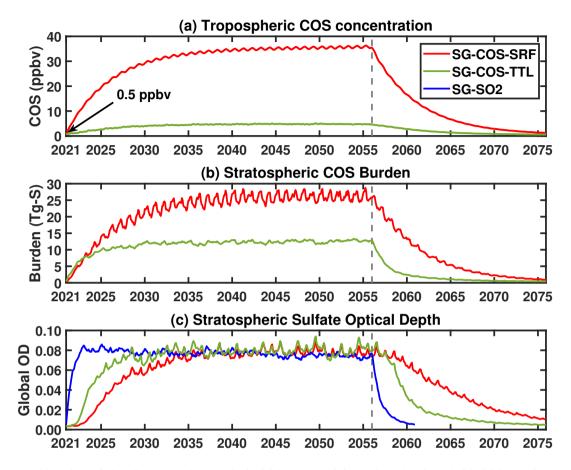
3.1 Sulfate burden

COS is the most abundant sulfur-containing species in the atmosphere under quiescent conditions (i.e. not considering explosive volcanic eruptions). It is efficiently lost at the surface via dry deposition on soils and vegetation: taking this sink into account, the net global lifetime (atmospheric chemistry plus surface deposition) is approximately 4 years, depending on the assumed magnitude of the soil and vegetation sink (Sandoval-Soto et al., 2005; Van Diest and Kesselmeier, 2008). In the troposphere the COS chemical reactivity (mostly with the hydroxyl radical) is rather slow: COS is thus well mixed and is easily transported in the stratosphere through the tropical tropopause layer (TTL). In the mid-stratosphere COS becomes efficiently photolyzed by solar UV radiation, becoming an important source for stratospheric SO_2 and finally for sulphuric acid aerosols.

When increasing the surface emission fluxes in SG-COS-SRF, it takes ~ 15 years before the concentration reaches a new equilibrium, from 0.5 to 35.5 ppbv (Fig. 2a), whereas in SG-COS-TTL the equilibrium value is 4.8 ppbv. In the same timespan, the global AOD increases reaching a value of 0.08 by 2035 in SG-COS-SRF and by 2030 in SG-COS-TTL, similar to the global value that is reached by the direct injection of SO_2 in the equatorial stratosphere in SG-SO2; in that case, however, the steady-state value is reached in only 1-2 years. In the GeoMIP G6sulfur experiment (Visioni et al. (2021b)), the average global surface cooling reported by 6 Earth system models for a similar stratospheric OD was 0.46 K. At the end of 2055, the increased COS and SO_2 injections are stopped. Average tropospheric COS concentrations follow an exponential decay guided by the atmospheric lifetime (3.8 years, due to chemistry but mainly soil deposition), reaching a value of 1.3 ppbv after 20 years in SG-COS-SRF (during 2075), whereas a similar value only takes 10 years to be reached in SG-COS-TTL. This means an increase of 0.8 ppbv with respect to background condition, that would produce a direct RF that is negligible compared to other well mixed greenhouse gases. The exponential decay of the stratospheric AOD in both SG-COS experiments is regulated by the stratospheric lifetime of COS (Fig. 2b), which is $\sim$10 years and it's mainly due to reaction with OH and photolysis, from which stratospheric SO_2 and finally sulphuric acid aerosols are formed. This is also combined with the depletion of the source

125 of COS from the troposphere (Fig. 2a). Therefore, the e-folding time for stratospheric AOD is longer with respect to the one resulting from SG-SO2 (Fig. 2c). In 2075, the global stratospheric AOD reaches a value of 0.01 in the SG-COS experiments with respect to 0.003 in the background case.

Figure 2. a) Monthly values of globally averaged tropospheric COS volume mixing ratio (ppbv) in both SG-COS experiments. The background value of 0.5 ppbv at the beginning of the simulation is highlighted. b) Monthly values of global stratospheric COS burden (in Tg-S) in both SG-COS experiments. c) Globally averaged stratospheric sulfate optical depth monthly values in SG-COS-SRF (red), SG-COS-TTL (green) and SG-SO2 (blue). The grey line in all panels indicates the time when emissions of COS and SO$_2$ are stopped, at the end of 2055.

3.2 Sulfate aerosol properties

	BG	SG-COS-SRF	SG-COS-TTL	SG-SO2	SG-COS-SRF - BG	SG-SO2 - BG
Total Sulfate OD	0.054±0.003	0.134±0.005	0.134±0.004	0.128±0.004	0.080±0.005	0.074±0.005
Tropospheric Sulfate OD	0.051±0.003	0.056±0.003	0.054±0.003	0.054±0.003	0.005±0.0054	0.003±0.004
Stratospheric Sulfate OD	0.003±0.001	0.078±0.002	0.080±0.004	0.074±0.001	0.075±0.002	0.071±0.001
Sulfate effective radius (μm)	0.18±0.01	0.46±0.01	0.47±0.01	0.59±0.01		
Ice OD	0.589±0.006	0.573±0.007	0.569±0.008	0.566±0.005	-0.016±0.008	-0.023±0.009
Ice effective radius (μm)	35±1	33±1	33±1	32±1		

Table 1. Summary of calculated sulfate aerosol and cirrus ice globally-annually averaged quantities relevant for RF calculations (i.e., optical depth at λ=0.55 μm and effective radius). Last two columns show the calculated SG changes with respect to the BG case [years 2046-2055].

In both COS experiments, COS emissions are adjusted so as to have the same global aerosol optical depth (AOD) $\approx$ 0.08 (see table 1). This is done in order to more easily compare the latitudinal distribution of the aerosols, and to better quantify the differences in the radiative forcing from both direct and indirect (ozone, methane and water vapor) changes in atmospheric composition.

There is a large difference in the latitudinal distribution of stratospheric sulfate optical depth, as shown in figure 3 (a). Both SG-COS experiments produce an AOD more uniformly distributed over all latitudes with respect to the SG-SO2 case, where the increase of optical depth is most prominent in the tropics; this is due to the efficient tropospheric mixing of COS before it reaches the stratosphere even when, as in SG-COS-TTL, the injection happens close to the tropopause.

The differences in the latitudinal distribution of AOD are also observable in the differences in the particle sizes and in the surface area density (SAD). Figure 3 (b) shows that the stratospheric effective radius is smaller in the SG-COS experiments and uniform for all latitudes, with a global value of 0.46 μm. In SG-SO2, the effective radius is higher in the tropics (0.59 μm); AOD is also larger in the tropics in that case, due to a larger concentration of particles there, even if larger particles are less effective at scattering incoming solar radiation (English et al., 2012).

Figure 4 shows a comparison of the effective radius (a) and SAD (b) between the BG, SG-COS-SRF, SG-COS-TTL and SG-SO2 cases, separating the tropics, mid-latitudes and polar regions. As SO$_2$ is injected at the equator, all oxidation and nucleation happens in the tropics in SG-SO2. This is reflected in the vertical distribution which has a maximum in the lowermost stratosphere. On the other hand in SG-COS, the effective radius increase is reached at higher altitudes, between 18-30 km, which is consistent with COS reaching higher altitudes through deep tropical convection before it is photochemically destroyed (Barkley et al., 2008). The same explanation is valid for the tropical SAD in panel (b).

As the size of the particles is determined by nucleation in the tropical region, where SO$_2$ oxidation occurs, mid-latitude and polar behaviour of the aerosols depends on the poleward transport by the Brewer-Dobson Circulation (BDC).

In SG-SO2, aerosols grow rapidly in the tropical region due to the high concentration of SO$_2$, and their larger size affects sedimentation rates, thus decreasing their lifetime. Consequently, the amount of aerosols transported to higher latitudes is

lower; in SG-COS, smaller particles with a higher lifetime are either easily transported towards the poles or directly formed there. Smaller particles at a higher concentration, and larger particles at a lower concentration may then result in a SAD which looks similar at mid-latitudes and polar region, but for different reasons.

155   The vertical distribution of particles and their optical properties are shown in Figure 5 (see Fig. S2 for COS, SO_2 and SO_4 concentration changes; only values for one of the SG-COS experiments is shown here, as they are indistinguishable). The vertical distribution of the SAD is fundamental to understand the role of the heterogeneous reaction and their effect on stratospheric ozone. The baseline case in panels (a) and (b) are a reference for understanding their changes in the SG-COS experiments (panels (c) and (d)). The particles transported via the BDC to the poles are large enough to efficiently scatter solar

160   radiation so that the SAD and extinction changes show a similar behaviour, with a global increase of stratospheric values with maxima at higher latitudes between 15-25 km.
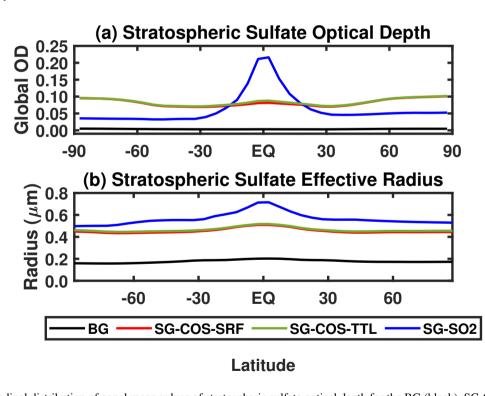
Panels (f) and (d) show the extinction and SAD changes between the three SG experiments, to underline that in SG-SO2 extinction of the radiation is confined in the tropical stratosphere between 15-25 km, meaning a negative change in SG-COS. As discussed before, the formation of larger particles in SG-SO2 in the tropical region reduces the amount of aerosol transported

165   to the poles compared to the SG-COS cases, where a larger number of smaller particles produces a positive change in SAD and, consequently, in extinction.
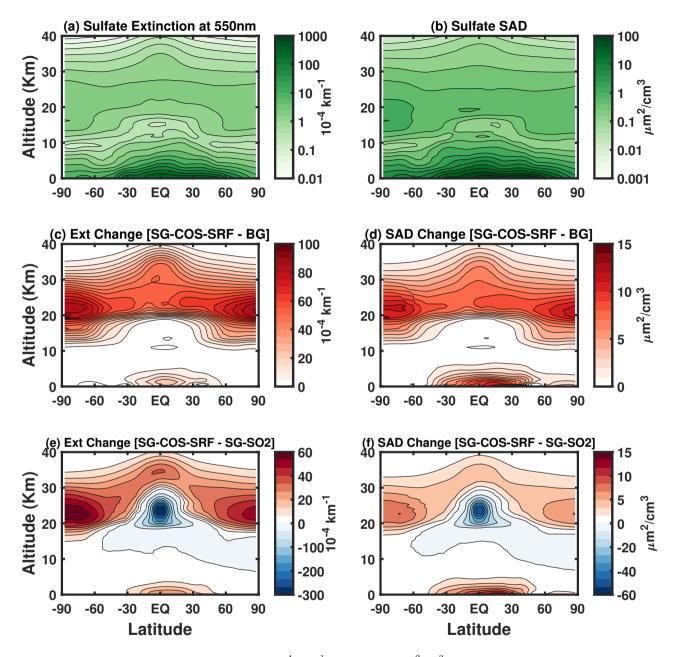
Figure 3. a) Latitudinal distribution of zonal mean values of stratospheric sulfate optical depth for the BG (black), SG-COS-SRF (red), SG-COS-TTL (green) and SG-SO2 (blue) cases. b) Stratospheric effective radius (in μm, from tropopause to 6hPa). All quantities are annually averaged over the years 2046-2055.

Figure 4. Vertical profiles of sulfate effective radius (in μm, a) and surface area density (in μm^2/cm^3, b) at different latitudinal bands (20N-20S for the Tropics, 30-50 at both N and S for the Mid-lat and 60-90 at both N and S for the Polar plots). All quantities are annually averaged over the years 2046-2055.

Figure 5. Zonal mean values of sulfate extinction (in 10^{-4} km^{-1}) and SAD (in μm^2/cm^3) in BG (panels a and b, respectively) and their change in the case of the SG-COS-SRF experiment (panels c and d). Panels e) and f) show extinction and SAD changes between SG-COS-SRF and SG-SO2. All quantities are annually averaged over the years 2046-2055.

3.3 Deposition

Experiment	MSA	SO$_2$	SO$_4$	COS	CS$_2$	H2S	Total
BG	1.0±0.1	35.2±1.4	9.4±0.4	0.39±0.01	0.47±0.03	1.5±0.1	48.0±1.8
SG-COS-SRF	1.0±0.1	36.4±1.5	9.9±0.4	31.6±0.1	0.47±0.03	1.5±0.1	80.9±1.7
SG-COS-TTL	1.0±0.1	35.8±1.5	9.7±0.4	3.5±0.1	0.47±0.03	1.5±0.1	52.0±1.7
SG-SO2	1.0±0.1	35.6±1.5	9.5±0.4	0.39±0.01	0.47±0.03	1.5±0.1	48.5±1.8

Table 2. Globally-annually averaged dry deposition rates of sulfur species (Tg-S/yr) [years 2046-2055].

Experiment	MSA	SO$_2$	SO$_4$	Total	Net [sources-sinks]
BG	1.5±0.1	3.0±0.1	43.2±1.5	47.7±1.6	+0.3±0.1
SG-COS-SRF	1.5±0.1	3.4±0.1	49.4±1.5	54.3±1.6	+0.8±0.1
SG-COS-TTL	1.5±0.1	3.2±0.1	45.2±1.5	49.9±1.6	+0.1±0.1
SG-SO2	1.5±0.1	3.2±0.1	46.5±1.5	51.2±1.6	+0.3±0.1

Table 3. Globally-annually averaged wet deposition rates of sulfur species (Tg-S/yr) [years 2046-2055]. The last column shows the net balance of total sulfur sources and sinks (Tg-S/yr).

The enhancement of the stratospheric sulfate burden would produce an increase in sulfur deposition, in dry form through acid gas deposition and in wet form through rain, fog and aerosol particles.

170   Acid deposition may damage human health when high concentrations of particles with a diameter below certain thresholds (PM2.5 and PM10) are inhaled. The acidification of soils and water may damage plants, microorganisms and aquatic animals, but the impact on the ecosystem depends on the rate at which acidifying compounds are deposited from the atmosphere, compared with the rate at which acid neutralizing capacity is generated within the ecosystem (Driscoll et al., 2001).

     Here we analyse how dry and wet deposition of sulfur species are distributed globally as a result of the two SG interventions.
175 Table 2 and 3 summarize wet and dry deposition rates for the SG-COS, SG-SO2 and BG experiments, and they include the contribution of each species to the total deposition. In particular, in both SG-COS experiments the increase in COS fluxes produces both an increase in sulfuric deposition, after its photolysis and oxidation to sulfuric acid, and in dry deposition of COS itself, as it is removed to the ground through uptake by vegetation and soils (Kettle et al., 2002).

     The global distribution of COS deposition for the baseline case is shown in figure 6(a) while the increase in deposition
180 from the SG-COS-SRF experiment is shown in figure 6(b). For the SG-COS-TTL case, the spatial distribution is identical to

SG-COS-SRF, but its magnitude is 10 times lower than in SG-COS-SRF. COS uptake by plants is concentrated mainly in the tropical rainforests of South America, Africa, and southeast Asia and boreal coniferous forests across North America, northern Europe, and northern Asia. Uptake by soils occurs mainly in arid and semiarid regions, such as savanna regions in the northern and southern Africa and in the southwestern regions of North America, in the pampas of Argentina, in Australia, and in the steppes of central Asia (Kettle et al., 2002). Dry deposition of COS doesn't contribute to acid deposition and, currently, there is no information available on how different soils or ecosystems would be affected by higher local COS concentrations; therefore, we assumed that their uptake efficiency does not change. The robustness of this assumption will need to be studied.

The global distribution of SO_x deposition is also shown in figure 6. Panels (c) and (d) show dry and wet deposition, respectively, for the background case. Dry deposition maxima are localized in urban areas close to the source where the emitted sulfur dioxide is immediately oxidized, while wet deposition distribution depends both on sulfate concentration and precipitation.

Panels (e) and (f) show the total SO_x deposition change in SG-COS-SRF with respect to the baseline case, in absolute terms and as a percentage of the baseline case, and most of its increase is due to wet deposition (see tables 2 and 3, and see Tables S1-4 for a breakdown of global sources and sinks of sulfur species). In both figures, the distribution of deposition is more uniform over the globe with respect to the tropical injection of SO_2, except for the polar regions, because of the reduced precipitation rates. Consequently, figure 6 (f) shows a large increase in percent deposition in the polar region (17% in the Arctic, 8% in Antarctic; these values are reduced to 1.7% and 0.8 % in SG-COS-TTL, see Fig. S4) because of very low values in the baseline case. On the other hand, deposition change is close to zero in polluted regions.
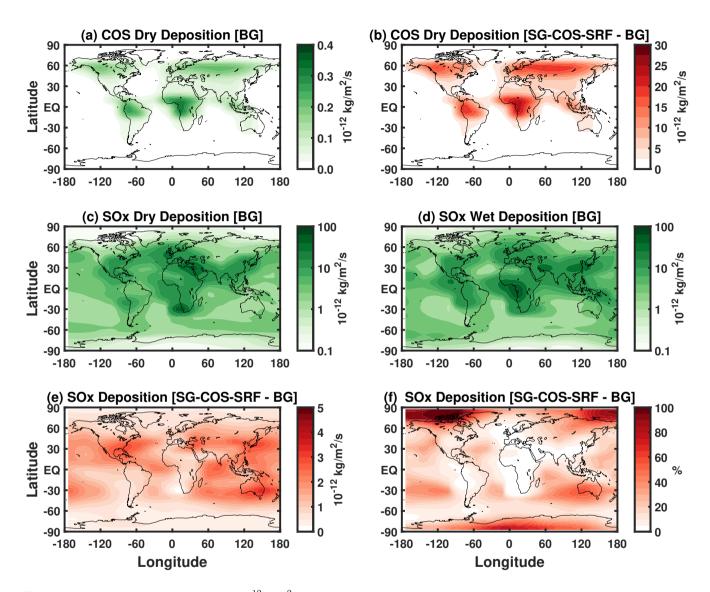
Globally, the annual differences in deposition fluxes for all species compared to the background case amount to 8.3 ± 0.2 Tg-S/yr for SG-COS-SRF, 3.1 ± 0.2 Tg-S/yr and 3.9 ± 0.2 Tg-S/yr for SG-SO2, which equates to an increase of 8.9 ± 0.3 %, 3.3 ± 0.3 % and 4.2 ± 0.3 %, respectively.

4 Indirect effects

	BG	SG-COS-SRF	SG-COS-TTL	SG-SO2	SG-COS-SRF - BG	SG-COS-TTL - BG	SG-SO2 - BG
COS [troposphere] (ppbv)	0.47±0.1	35.5±0.2	4.8±0.1	0.47±0.1	35.0±0.2	4.3±0.2	0.00±0.1
CH$_4$ lifetime (yr)	8.72±0.13	9.83±0.18	9.85±0.17	9.78±0.20	1.11±0.13 [(+12.7±1.4) %]	1.13±0.13 [(+13.0±1.4) %]	1.06±0.17 [(+12.2±2.0) %]
H$_2$O [stratosphere] (ppmv)	6.08±0.08	5.99±0.16	5.95±0.15	6.13±0.13	-0.09±0.14	-0.13±0.15	0.05±0.12
O$_3$ column (DU)	289.3±1.8	294.2±1.5	294.8±1.6	290.7±1.6	4.9±2.3	5.5±2.4	1.4±1.7

Table 4. Summary of calculated globally-annually averaged quantities of greenhouse gases directly and indirectly perturbed by SG and relevant for RF calculations (i.e., COS mean tropospheric mixing ratio, CH$_4$ atmospheric lifetime, H$_2$O mean stratospheric mixing ratio, O$_3$ column). Last two columns show the calculated SG changes with respect to the BG case [years 2046-2055].

Figure 6. a) Surface dry deposition fluxes (10^{-12}kg/m^2/s) of COS in the background case. b) Change in COS dry deposition fluxes in SG-COS-SRF compared to a). c) SO$_x$ dry deposition fluxes (10^{-12}kg/m^2/s) in the background case. d) SO$_x$ dry deposition fluxes (10^{-12}kg/m^2/s) in the background case. e) Change in SO$_x$ total deposition fluxes in SG-COS-SRF compared to the background. f) as e) but in % of the background values.

	BG (W/m^2)	SG-COS-SRF (W/m^2)	SG-COS-TTL (W/m^2)	SG-SO2 (W/m^2)	SG-COS-SRF - BG (%)	SG-COS-TTL - BG (%)	SG-SO2 - BG (%)
UVB	0.206±0.002	0.197±0.001	0.196±0.001	0.201±0.001	-4.4±0.6	-5.8±0.6	-2.4±0.9
UVA	11.35±0.01	11.13±0.01	11.12±0.01	11.17±0.01	-1.9±0.1	-2.0±0.1	-1.6±0.1

Table 5. Summary of calculated globally-annually averaged quantities of UVB and UVA at surface. Last two columns show the calculated SG percentage changes with respect to the BG case [years 2046-2055].

The simulated enhancement in the stratospheric aerosol layer would produce two main effects: an increased scattering of solar radiation, that in turn would reduce surface temperatures, and the local absorption of more near-infrared solar and terrestrial radiation, that would warm the stratospheric layer where the aerosols reside (as observed for volcanic eruptions, see Lacis et al., 1992; Labitzke and McCormick, 1992). Furthermore, the increase in the surface area density of the aerosols would affect the heterogeneous chemistry of ClO_x and NO_x with implications for ozone concentration and UV radiation at the surface (Tilmes et al., 2009, 2018b, 2021).

For SO_2, it has been shown that the combination of surface cooling, perturbation of stratospheric temperatures and changes in tropospheric ozone and in UV at the surface also affects methane lifetime (Visioni et al., 2017a). In this section we analyse the differences in these changes also for the SG-COS experiment.

Figure 7 shows the ozone changes in SG-COS-SRF and SG-SO2 with respect to the BG case (SG-COS-TTL is equivalent to SG-COS-SRF). Panels (a) and (b) show the monthly total ozone column changes as a function of latitude. Close to the equator there is a small reduction in the overall column, mostly due to a reduction in tropospheric ozone, as visible in panels (c) and (d), as a direct consequence of the surface cooling (Nowack et al., 2016). On the other hand, at higher latitudes an overall increase in the total column is observable due to an increase in stratospheric ozone. This is particularly evident closer to the poles.

During springtime months, there is some Antarctic ozone depletion, while in the Arctic a recovery of ozone is observable. In the Antarctic spring, the polar vortex is strengthened by the stratospheric heating in the tropics that affects the equator-to-pole thermal wind balance (Visioni et al., 2020), resulting in greater confinement of cold air, that, in turn, enhances the ozone depletion by the polar stratospheric clouds (PSC). The tropical stratospheric heating is higher in SG-SO2 with respect to SG-COS as the aerosols are less confined (fig. S6). Consequently, the strengthening of polar vortex in SG-SO2 produces a higher ozone depletion. In the Arctic, on the other hand, PSC-related ozone loss is lower (Tilmes et al., 2018a), and the predominant effect is that from an acceleration of the BDC transporting ozone-rich air from lower latitudes.

Panels (c) and (d) show the annual mean of ozone mixing ratio percentage change as a function of altitude and latitude. In both SG experiments, negative changes below the tropopause are governed by the decrease in solar radiation which comes into play in the photo-dissociation reaction of NO_x as an ozone precursor (NO_2 + hν ($\lambda < 420$ nm) $\rightarrow$ NO + O(^{3}P)). Sunlight reduction also affects the O_3 photolysis, decreasing the ozone loss. Positive changes are due to the balance of the previous reactions and the increase of methane (see table 4) as a source of ozone in its oxidation chain, and mainly due to the decrease of the tropospheric water vapour in a clean air environment (low NO_x), such as the tropics (Nowack et al., 2016; Xia et al., 2017b).

230   Above the tropopause, there is a negative ozone change in the lower stratosphere in all SG experiments, except for the Arctic region where we observe a small increase in the Arctic lowermost stratosphere in all cases. The key drivers of stratospheric ozone change are the increase in heterogeneous reactions, as a result of the enhancement of stratospheric aerosols, and the perturbation of the dynamics governing ozone transport.

Negative ozone changes correspond to the region where the SAD reaches its maximum values (fig. 5 (d) and (f)): between
235   10-20 km in the polar regions for SG-COS and mainly between 15-25 km at tropics for SG-SO2. The increase of the SAD enhances heterogeneous chemistry and results in denitrification via hydrolysis of dinitrogen pentoxide ($N_2O_5 + H_2O \xrightarrow{M}$ $2HNO_3$). The loss of NO_x decreases the rate of ozone depletion through its catalytic cycle. Whereas in the mid-stratosphere, where the cycles of chlorine (ClO_x) and bromine (BrO_x) are dominant, there is an increase in ozone loss since reduction of NO_x, that normally bounds chlorine ($ClONO_2$), allows ClO to destroy more ozone (Tilmes et al., 2018b; Grant et al., 1992).

240   At low latitudes, stratospheric ozone concentration is also driven by changes in tropical upwelling (Visioni et al., 2021a): the reduction in tropical upwelling of ozone-poor air coming from the lowermost stratosphere leads to higher ozone concentration at altitudes of about 20-22 km (Tilmes et al., 2018b).

Figure S7 (e) shows the change of tropical upwelling in relation to changes in the residual vertical velocity (w*) with respect to the baseline case. Negative w* anomalies in SG-COS mean weaker tropical upwelling as consequence of tropospheric
245   cooling. In SG-SO2, the highest concentration of absorbing aerosols leads to positive w* above 20 km due to the local warming but this doesn't affect the transport of ozone-poor air from the lower layers.

Above the discussed altitudes, there is a net ozone production in all SG experiments, with an higher increase of ozone mixing ratio in SG-COS experiment with respect to SG-SO2, especially in the extra-tropical region. Ozone depletion at these altitudes is mainly controlled by the catalytic cycle of NO_x, that is inhibited by the denitrification process due to heterogeneous reactions
250   on aerosols.

Globally, the annually-averaged ozone column increases of ∼5 and 1.5 DU for SG-COS and SG-SO2, respectively (table 4). Increasing stratospheric ozone affects UVB at the surface because it is absorbed by ozone during its photodissociation, while aerosol could affect UVA radiation by scattering processes: the projected changes are shown in figure 8 for both UVA and UVB for each season and for the annual mean. We estimated these changes using TUV (from https://www2.acom.ucar.edu/
255   modeling/tropospheric-ultraviolet-and-visible-tuv-radiation-model), using in input our model latitudinal and monthly values for the period (2046-2055) for aerosol optical depth, total ozone column, climatological cloud cover and surface albedo.

In all SG experiments, the negative changes of UVB radiation at surface, except in the Antarctic region, are related to the variation in stratospheric ozone. as well as the interannual variation that increase towards the poles, due to the seasonal variation of ozone, as discussed before. UVA decreases everywhere in all SG experiments. In particular, the correlation between UVA
260   change and particles scattering is evident if we compare this latitudinal distribution with the stratospheric AOD of figure 3(a). The globally averaged UVB and UVA changes at surface are summarized in table 5.
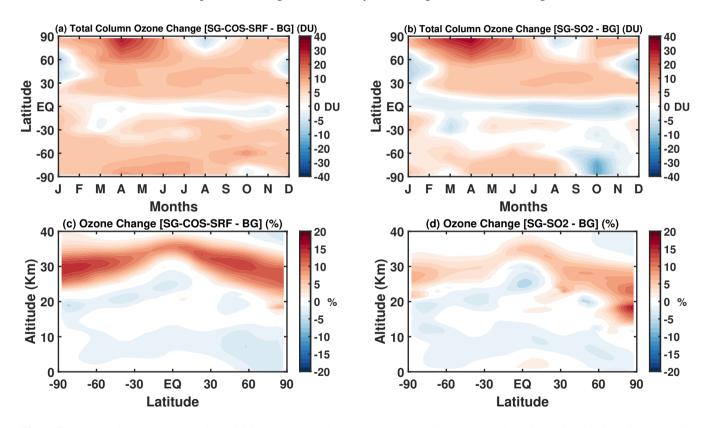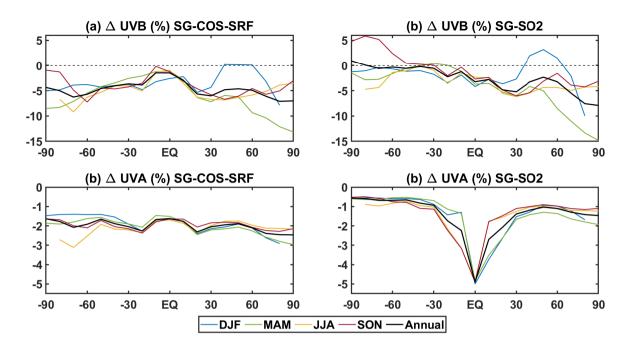
Methane is an indirect source of tropospheric ozone (West and Fiore, 2005), and it is also a greenhouse gas. Knowing its variation is fundamental to understand the final contribution to the radiative forcing that one would wish to achieve with this geoengineering method. From table 4, we find a global increase in methane lifetime of ∼ 13% in SG-COS and 12.2% in

265   SG-SO2, which we can identify in the increase in methane itself. The reason for the increase in methane is to be found in the behaviour of the hydroxyl radical (OH), as the main sink of methane is the oxidation reaction with OH: decrease of OH means an increase of methane lifetime. As discussed by Visioni et al. (2017b), mechanisms that cause an increase in OH are as follows: (a) surface cooling lessens the amount of tropospheric water vapor and inhibits the temperature-dependent reaction of NO + O_3; (b) decrease of tropospheric UV, due to enhancement of ozone and scattering radiation, reduce $O(^1D)$ that takes

270   part of the reaction $O(^1D) + H_2O \rightarrow 2$ OH; (c) increase of SAD enhances heterogeneous chemistry reducing the amount of NO_x (NO + HO_2, NO + RO_2); (d) increase of tropical lower stratosphere temperature (TTL) that regulates the stratosphere-troposphere exchange, which can be positive or negative depending on the net result of the superimposed species (CH_4, NO_y, O_3, SO_4) in the extratropical upper troposphere-lower stratosphere (UTLS).

The warming of the TTL is shown in figure S7 (d): in SG-SO2, larger particles confined in the tropical region produce a

275   greater warming of the TTL with respect to smaller ones distributed all over the globe in SG-COS. The role of dimensions and distributions of aerosols in stratospheric warming is confirmed by the heating rates, as shown in figure S6.

Figure 7. a,b) Monthly mean zonal values of SG ozone total column changes (DU) with respect to the BG case for SG-COS-SRF and SG-SO2 respectively. c, d) ozone mixing ratio percent changes with respect to the BG case. All quantities are annually averaged over the years 2046-2055.

Figure 8. Zonal UVB and UVA surface changes per each season in percentage with respect to BG case in SG-COS-SRF (panels a and b, respectively) and SG-SO2 (panels c and d). All quantities are averaged over the years 2046-2055.

5 Radiative forcing

Total RF (W/m^2)	SW	LW	NET
SG-COS-SRF	-1.47±0.12	+0.21±0.25	-1.26±0.13
SG-COS-TTL	-1.41±0.12	-0.06±0.25	-1.47±0.13
SG-SO2	-1.58±0.10	-0.11±0.23	-1.69±0.13

Table 6. Globally-annually averaged total RF of sulfate aerosols and greenhouse gases for the SG experiments with respect to BG (shortwave, longwave and net) (W/m^2) [years 2046-2055].

The ULAQ-CCM radiative transfer module calculates online the radiative forcing due to aerosols, greenhouse gases (GHGs), and low and high clouds. The effects of single components have been estimated offline for both shortwave (SW) and longwave (LW) with the same radiative transfer core, for sulfate aerosols, clouds, COS, CH_4, stratospheric H_2O, stratospheric and tropospheric O_3 in order to properly separate the contributions.

Tables S8, S9 and S10 summarise the individual contributions of GHGs changes for SG-COS-SRF, SG-COS-TTL and SG-SO2, respectively. Similar increases of methane in all SG experiments produce the same positive LW RF; the TTL warming

(which results in an increase in stratospheric water vapor), results in a small but positive contribution from H_2O in SG-SO2.
Contributions from both stratospheric and tropospheric O_3 changes have also been estimated, but are negligible.

In both SG-COS experiments, obviously, the increase of COS concentration, which is a GHG, must be taken into account. We estimated its contribution to the radiative forcing based on the definition of global warming potential (GWP) on a mass/mass basis as in Brühl et al. (2012) for a time horizons of 30 years (2021-2050). GWP can be approximated as follows by the expression of Roehl et al. (1995), assuming that the perturbation of the radiation balance of the Earth by greenhouse gases COS and CO_2 decays exponentially after a pulse emission for a time horizon ΔT.

$$GWP_{\Delta t} \simeq \frac{RF_{COS}}{RF_{CO_2}} \times \frac{\tau_{COS}}{\tau_{CO_2}} \times \frac{1 - e^{\frac{-\Delta_t}{\tau_{COS}}}}{1 - e^{\frac{-\Delta_t}{\tau_{CO_2}}}} \tag{1}$$

We assumed an overall lifetime of τ_{COS}=3.8 yr and τ_{CO_2}=75 yr, and the radiative forcing of 1 kg of COS relative to 1 kg of CO_2 added to the present atmosphere (RF_{COS}/RF_{CO_2}) is 724 (Brühl and Crutzen, 1988). This results in a GWP of 111. For our time period, the mass of COS and CO_2 added to the atmosphere (Δm) is 1.97×10^{12} kg of COS (for SG-COS-SRF), 0.35 $\times 10^{12}$ kg of COS (for SG-COS-TTL) and 1.23×10^{15} kg of CO_2. Therefore, the COS radiative forcing can be calculated as:

$$RF_{COS} = GWP_{\Delta t} \times RF_{CO_2} \times \frac{\Delta m_{COS}}{\Delta m_{CO_2}} \tag{2}$$

where RF_{CO_2} in RCP6.0 is estimated to be 0.83 W/m^2 considering an increase of 68.5 ppm from a baseline of 409.2 ppm. Overall, this results in a radiative forcing from the COS increase of 0.17 W/m^2 in SG-COS-SRF and of 0.03 W/m^2 in SG-COS-TTL.
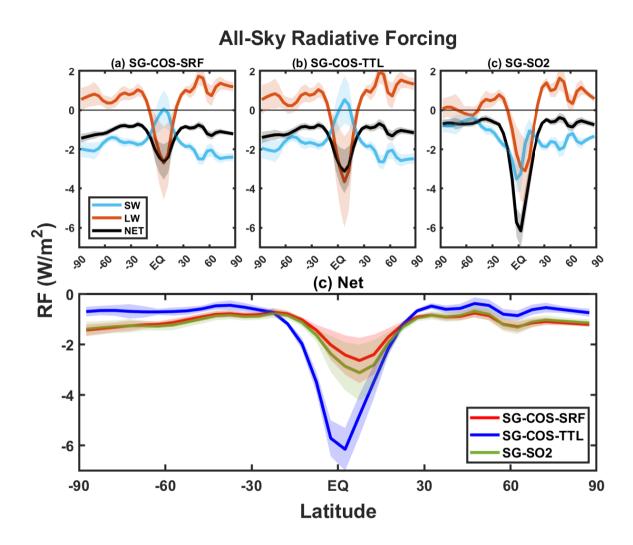
The main contributions of sulfate aerosols and clouds are summarised in tables S5, S6 and S7 for SG-COS-SRF, SG-COS-TTL and SG-SO2, respectively. The contribution of sulfate aerosols is the sum of the cooling effects given by the efficient scattering of solar radiation by particles of radius of around 0.5 μm and the absorption of LW by larger ones. Globally, the estimated values are similar for the Clear-Sky SW and LW forcing from the sulfate aerosols: in terms of the latitudinal distribution, however, SG-SO2 presents a peak in the tropics whereas the forcing from SG-COS is much more latitudinally even.

The reduction in optical depth from cirrus clouds (see table 1) produced by the aerosols (Kuebbeler et al., 2012; Visioni et al., 2018a) results in a net negative radiative forcing. This is given by the balance between the positive RF in the shortwave (SW) due to the reduction of reflected solar radiation and the negative RF in the longwave (LW) due to the decrease of trapped planetary radiation, which reduces the contribution to the greenhouse effect. In the SG-COS cases, at the equator the positive RF from the thinning locally balances the direct forcing from the aerosol (figures 9 and S8).

Table 6 summarises the total contribution of sulfate aerosols and greenhouse gases under All-Sky conditions.

All-Sky Radiative Forcing

Figure 9. a-c) Mean zonal shortwave (cyan), longwave (orange), and net (black) All-Sky radiative forcing (in W/m²) in SG-COS-SRF, SG-COS-TTL and SG-SO2 respectively. d) Comparison of the net radiative forcings from SG-COS-SRF (red), SG-COS-TTL (green) and SG-SO2 (blue). All quantities are annually averaged over the years 2046-2055. Shadings in all panels represent 1 standard deviation in the interannual variability.

6 Technical feasibility of SG through COS emissions

We briefly discuss here the technical feasibility of the approach described in this paper, as mainly related to the increase of surface COS emissions (for SO_2 injections, see for instance Smith and Wagner, 2018; Smith et al., 2020).

Patent number 3,409,399 (1968) has developed a method for high yield synthesis of COS (93.2-96.6%):

$$CO_2 + CS_2 \xrightarrow{\quad 100-600^\circ C \quad} 2COS$$

CO_2 is abundant even in concentrated (90%+) streams, from various natural and industrial sources, particularly with co-operation from states or industries. For example, capturing flue gas from coal-fired power plants is an established technology and may yield over 90% CO_2 (Wang et al., 2013). CS_2 is produced via numerous means, perhaps the easiest being from coke (carbon) and molten sulfur:

$$C + 2S \xrightarrow{\quad \text{high temperature} \quad} CS_2$$

Approximately 1 million tons of CS_2 is produced per year (Madon and Strickland-Constable, 1958), with China consuming approximately half of the global production of CS_2 for rayon manufacturing. CS_2 is highly unstable and is flammable in air. It is also toxic at low concentrations (10 ppm).

Given the reactions above, about 0.5 Tg of S will produce 0.94 Tg of COS: this amounts to 0.16 Tg of C (coke) and 0.55 Tg of molten sulfur. In the last decade, approximately 70 Tg of sulfur were produced worldwide, so this would constitute an increase in S production of 0.8%. The price varied between $50 and $200 per ton, leading to an annual cost of approximately $25-100 million. Worldwide production of coke was around 640 Tg, so this increase in production is negligible. The price of coke varies between $50 and $100 per ton, leading to an annual cost of approximately $8-16 million. To this we would have to add the cost of CO_2, as well as the production and energy costs. Considering an estimate of $400 million per year for each Tg of S between CO_2 and production and energy cost, and assuming an effort shared between 1000 locations, this would add up to $400.000 per location per year per each Tg of S. The overall cost is roughly of the same order of magnitude as that in Smith and Wagner (2018) for a stratospheric aerosol deployment at ~ 20 km of injection (so different from the injection set-up in our study for SG-SO2), but without the need to develop a new aircraft-based delivery system. For the SG-COS-TTL case, the overall cost would be a combination of the production costs of COS as described above (but almost 10 times less per year to obtain the same AOD as SG-COS-SRF) and those of a deployment in the upper troposphere, which may result to be less expensive than a deployment in the lower stratosphere as needed for SO_2.

 7 Conclusions

We have presented here the results of a modeling experiment with the aim of producing an optically thick cloud of sulfate aerosols in the stratosphere without the injection of sulfate precursors directly in the stratosphere, but rather using increased surface or upper tropospheric emissions of carbonyl sulfide (COS). The low reactivity of COS in the troposphere, where it is not reactive and where it is predominantly absorbed by some soils and by plants, allows for a large portion of its emissions to
345 reach the stratosphere, where it is turned into sulfate aerosols by photo-dissociation and oxidation.

We compare the results obtained in the following injection scenarios: i) 40 Tg-S/yr of COS injected from the surface (roughly 400 times more than the background emissions); ii) 6 Tg-S/yr of COS injected in the equatorial upper troposphere (15 km); iii) 4 Tg-S/yr of SO_2 injected in the equatorial stratosphere as prescribed in previous experiments (Kravitz et al., 2011; Visioni et al., 2017a). All experiments result in a similar global optical depth from the produced stratospheric aerosols (~ 0.08), but
350 with different latitudinal distributions: for SO_2, as previously observed in various modeling experiments, equatorial injections result in an increased concentration of aerosols in the tropical stratosphere that tends to overcool the tropics and undercool the high latitudes (Kravitz et al., 2018; Jiang et al., 2019), while also reducing the efficacy of the back-scattering from the aerosols due to the increased size of the particles (Visioni et al., 2018c). On the other hand, with COS emissions, independently from the injection height, the uniform mixing of the gas allows for a more uniform distribution of the produced aerosols in the
355 stratosphere, resulting in increased optical depth also at very high latitude.

The differences in distribution and size of the particles result in different changes to the composition of the atmosphere: smaller particles absorb and heat the stratosphere less, thus resulting in fewer dynamical changes. From a chemical perspective, stratospheric ozone would be impacted differently from the two geoengineering schemes. For SO_2 injections, previous studies have shown that the overall effect is the result of a combination of various dynamical and chemical factors that behave
360 differently depending on the latitude and altitude of the aerosols. At low latitudes the increase in lower stratospheric water vapor produced by the warming of the tropopause layer enhances the halogen-driven destruction of ozone in the lower stratosphere (Tilmes et al., 2018b) due to NO_x depletion. This effect is balanced by reduced ozone destruction in the middle stratosphere due to the slowing down of the NO_x cycle produced by enhanced heterogeneous chemistry (Pitari et al., 2014; Richter et al., 2017; Franke et al., 2021).
365 Overall, in the case of COS emissions the further increase in surface area density produced by smaller particles increases the inhibition of the ozone cycles in the middle stratosphere, resulting in a net increase in stratospheric ozone and thus in a larger decrease of UV radiation at the surface. Similarly, the larger sulfate burden at high latitudes produces further ozone recovery and thus less UV radiation also at the poles for the COS case.

Our results point to the feasibility of increased emissions of COS as a possible substitute to stratospheric SO_2 (or other
370 sulfate precursors) injections to produce stratospheric sulfate aerosols. Surface emissions would sidestep the problem of deploying methods not already available to bring the sulfate at those altitudes, including development of novel aircraft (Bingaman et al., 2020). Since COS is already a byproduct of human activities, it might be possible to devise methods of mass-production of the required quantities that may be cheaper than the known proposed methods (Smith et al., 2020). However, this strategy

necessitates a larger amount of emissions to achieve the same global stratospheric AOD, resulting in larger amounts of de-
position. Furthermore, while the toxic levels of COS concentrations are orders of magnitude larger than the one achieved in
our simulation (Kilburn and Warshaw, 1995; Bartholomaeus and Haritos, 2006), the effects of prolonged exposure to lower
concentrations would have to be assessed; the effect of increased COS concentrations on ecosystems would also require careful
investigation. Estimations of the tropospheric radiative effect would also need to be refined to make sure that it is not larger
than previously estimated, reducing the efficacy of the aerosol-induced cooling. We have shown that tropospheric injections
of lower quantities of COS would produce the same optical depth and indirect effects while resulting in an increase in tropo-
spheric COS concentrations 10 times lower than with surface emissions. This would however still require the deployment of an
aircraft fleet as in SO_2 emissions, but the technical challenges of reaching 15 km might be less than those faced when reaching
20 km Smith et al. (2020).

Overall, there may be other weak points in geoengineering strategies using COS emissions compared to SO_2 that need to be
addressed. They would be less easily scalable, and both deployment and phase-out, as we have shown, would require a longer
time-frame compared to the almost instantaneous effect produced by SO_2 injections. Considering the dangers to ecosystems
presented by a too fast deployment or termination of sulfate geoengineering (Trisos et al., 2018), this might not actually be a
large drawback, but it does remove the possibility of rapidly "regulating" the necessary amount of stratospheric sulfate in case
of changes in strategy or external conditions (such as a Pinatubo-like volcanic eruption; Laakso et al., 2016). The comparison
between our two COS experiments suggest that the mixing happening in the troposphere would not allow any control in the
latitudinal or seasonal distribution of the resulting aerosols, as proposed elsewhere for SO_2 injections (MacMartin et al., 2017;
Dai et al., 2018; Visioni et al., 2019); however, future investigations may expand on this work by exploring if a different
combination of injection altitudes and locations may offer at least some control over the aerosol cloud.

Clearly, this study is intended to be just a pilot study of this method, and further simulations with other climate models,
possibly with a coupled ocean and interactive land model to determine the full surface response, are needed. The agreement
between the baseline results presented here and the information present in the literature point to a robustness of our results,
but further studies are required to understand different aspects of the climate response: for instance, studies would need to
investigate the possible response of vegetation and soils to the increased concentration of COS in the troposphere, and if the
efficacy of the sinks would change due to shifts in temperature and precipitation produced by both climate change and the
intervention.

Overall, however, the results obtained in this work show that, as a geoengineering technique, emissions of carbonyl sulfide
should be further studied and considered by the scientific community as a possible alternative to the others already studied in
the literature.

Data availability. Data used in this work will be made available through the Cornell eCommons platform before publication.

405 *Author contributions.* DV and GP devised the study. IQ ran the simulations, analysed the results, produced the figures and wrote the manuscript with the assistance of DV. BK wrote Section 6 and contributed to the final draft of the manuscript.

Competing interests. The authors declare no competing interests

Acknowledgements. Support for B.K. was provided in part by the National Science Foundation through agreement CBET-1931641, the Indiana University Environmental Resilience Institute, and the *Prepared for Environmental Change* Grand Challenge initiative. Support for 410 D.V. was provided by the Atkinson Center for a Sustainable Future at Cornell University.

References

Barkley, M. P., Palmer, P. I., Boone, C. D., Bernath, P. F., and Suntharalingam, P.: Global distributions of carbonyl sulfide in the upper troposphere and stratosphere, Geophysical Research Letters, 35, https://doi.org/https://doi.org/10.1029/2008GL034270, 2008.

Bartholomaeus, A. and Haritos, V.: Review of the toxicology of carbonyl sulfide, a new grain fumigant, Food and chemical toxicology : an international journal published for the British Industrial Biological Research Association, 43, 1687–701, https://doi.org/10.1016/j.fct.2005.06.016, 2006.

Bingaman, D. C., Rice, C. V., Smith, W., and Vogel, P.: A Stratospheric Aerosol Injection Lofter Aircraft Concept: Brimstone Angel, in: AIAA Scitech 2020 Forum, AIAA SciTech Forum, American Institute of Aeronautics and Astronautics, https://doi.org/10.2514/6.2020-0618, 2020.

Brühl, C. and Crutzen, P. J.: Scenarios of possible changes in atmospheric temperatures and ozone concentrations due to man's activities, estimated with a one-dimensional coupled photochemical climate model, Climate Dynamics, 2, 173–203, https://doi.org/10.1007/BF01053474, 1988.

Brühl, C., Lelieveld, J., Crutzen, P. J., and Tost, H.: The role of carbonyl sulphide as a source of stratospheric sulphate aerosol and its impact on climate, Atmospheric Chemistry and Physics, 12, 1239–1253, 2012.

Budyko, M. I.: Climatic Changes, Volume 10, American Geophysical Union, https://doi.org/DOI:10.1029/SP010, 1977.

Conrad, R. and Meuser, K.: Soils contain more than one activity consuming carbonyl sulfide, Atmospheric Environment, 34, 3635–3639, 2000.

Crutzen, P. J.: The possible importance of CSO for the sulfate layer of the stratosphere, Geophysical Research Letters, 3, 73–76, https://doi.org/https://doi.org/10.1029/GL003i002p00073, 1976.

Crutzen, P. J.: Albedo Enhancement by Stratospheric Sulfur Injections: A Contribution to Resolve a Policy Dilemma?, Climatic Change, 77, 211–220, https://doi.org/10.1007/s10584-006-9101-y, 2006.

Dai, Z., Weisenstein, D. K., and Keith, D. W.: Tailoring Meridional and Seasonal Radiative Forcing by Sulfate Aerosol Solar Geoengineering, Geophysical Research Letters, 45, 1030–1039, https://doi.org/10.1002/2017GL076472, 2018.

Driscoll, C. T., Lawrence, G. B., Bulger, A. J., Butler, T. J., Cronan, C. S., Eagar, C., Lambert, K. F., Likens, G. E., Stoddard, J. L., and Weathers, K. C.: Acidic Deposition in the Northeastern United States: Sources and Inputs, Ecosystem Effects, and Management Strategies: The effects of acidic deposition in the northeastern United States include the acidification of soil and water, which stresses terrestrial and aquatic biota, BioScience, 51, 180–198, https://doi.org/10.1641/0006-3568(2001)051[0180:ADITNU]2.0.CO;2, 2001.

Eastham, S. D., Weisenstein, D. K., Keith, D. W., and Barrett, S. R.: Quantifying the impact of sulfate geoengineering on mortality from air quality and UV-B exposure, Atmospheric Environment, 187, 424 – 434, https://doi.org/https://doi.org/10.1016/j.atmosenv.2018.05.047, 2018.

Eichinger, R., Dietmuller, S., Garny, H., Sacha, P., Birner, T., Bonisch, H., Pitari, G., Visioni, D., Stenke, A., Rozanov, E., Revell, L., Plummer, D. A., Jockel, P., Oman, L., Deushi, M., Kinnison, D. E., Garcia, R., Morgenstern, O., Zeng, G., Stone, K. A., and Schofield, R.: The influence of mixing on the stratospheric age of air changes in the 21st century, Atmospheric Chemistry and Physics, 19, 921–940, 2019.

English, J. M., Toon, O. B., and Mills, M. J.: Microphysical simulations of sulfur burdens from stratospheric sulfur geoengineering, Atmospheric Chemistry and Physics, 12, 4775–4793, 2012.

Eyring, V., Butchart, N., Waugh, D. W., Akiyoshi, H., Austin, J., Bekki, S., Bodeker, G. E., Boville, B. A., Brühl, C., Chipperfield, M. P., Cordero, E., Dameris, M., Deushi, M., Fioletov, V. E., Frith, S. M., Garcia, R. R., Gettelman, A., Giorgetta, M. A., Grewe, V., Jourdain, L., Kinnison, D. E., Mancini, E., Manzini, E., Marchand, M., Marsh, D. R., Nagashima, T., Newman, P. A., Nielsen, J. E., Pawson, S., Pitari, G., Plummer, D. A., Rozanov, E., Schraner, M., Shepherd, T. G., Shibata, K., Stolarski, R. S., Struthers, H., Tian, W., and Yoshiki, M.: Assessment of temperature, trace species, and ozone in chemistry-climate model simulations of the recent past, Journal of Geophysical Research, 111, D22 308, https://doi.org/10.1029/2006JD007327, 2006.

Franke, H., Niemeier, U., and Visioni, D.: Differences in the quasi-biennial oscillation response to stratospheric aerosol modification depending on injection strategy and species, Atmospheric Chemistry and Physics, 21, 8615–8635, 2021.

Grant, W., Fishman, J., Browell, E., Brackett, V., Nganga, D., Minga, A., Cros, B., Veiga, R. E., Butler, C., Fenn, M., and Nowicki, G.: Observations of reduced ozone concentrations in the tropical stratosphere after the eruption of Mt. Pinatubo, Geophysical Research Letters, 19, 1109–1112, 1992.

Institute of Medicine and National Academy of Sciences and National Academy of Engineering: Policy Implications of Greenhouse Warming: Mitigation, Adaptation, and the Science Base, The National Academies Press, Washington, DC, https://doi.org/10.17226/1605, 1992.

Jiang, J., Cao, L., MacMartin, D. G., Simpson, I. R., Kravitz, B., Cheng, W., Visioni, D., Tilmes, S., Richter, J. H., and Mills, M. J.: Stratospheric Sulfate Aerosol Geoengineering Could Alter the High-Latitude Seasonal Cycle, Geophysical Research Letters, 46, 14 153–14 163, https://doi.org/10.1029/2019GL085758, 2019.

Kettle, A. J., Kuhn, U., von Hobe, M., Kesselmeier, J., and Andreae, M. O.: Global budget of atmospheric carbonyl sulfide: Temporal and spatial variations of the dominant sources and sinks, Journal of Geophysical Research: Atmospheres, 107, ACH 25–1–ACH 25–16, https://doi.org/https://doi.org/10.1029/2002JD002187, 2002.

Khalil, M. and Rasmussen, R.: Global sources, lifetimes and mass balances of carbonyl sulfide (OCS) and carbon disulfide (CS2) in the earth's atmosphere, Atmospheric Environment (1967), 18, 1805–1813, 1984.

Kilburn, K. H. and Warshaw, R. H.: Hydrogen Sulfide and Reduced-Sulfur Gases Adversely Affect Neurophysiological Functions, Toxicology and Industrial Health, 11, 185–197, 1995.

Kravitz, B., Robock, A., Boucher, O., Schmidt, H., Taylor, K. E., Stenchikov, G., and Schulz, M.: The Geoengineering Model Intercomparison Project (GeoMIP), Atmospheric Science Letters, 12, 162–167, https://doi.org/10.1002/asl.316, 2011.

Kravitz, B., Rasch, P. J., Wang, H., Robock, A., Gabriel, C., Boucher, O., Cole, J. N. S., Haywood, J., Ji, D., Jones, A., Lenton, A., Moore, J. C., Muri, H., Niemeier, U., Phipps, S., Schmidt, H., Watanabe, S., Yang, S., and Yoon, J.-H.: The climate effects of increasing ocean albedo: an idealized representation of solar geoengineering, Atmospheric Chemistry and Physics, 18, 13 097–13 113, https://doi.org/10.5194/acp-18-13097-2018, 2018.

Kuai, L., Worden, J. R., Campbell, J. E., Kulawik, S. S., Li, K.-F., Lee, M., Weidner, R. J., Montzka, S. A., Moore, F. L., Berry, J. A., Baker, I., Denning, A. S., Bian, H., Bowman, K. W., Liu, J., and Yung, Y. L.: Estimate of carbonyl sulfide tropical oceanic surface fluxes using Aura Tropospheric Emission Spectrometer observations, Journal of Geophysical Research: Atmospheres, 120, 11,012–11,023, https://doi.org/https://doi.org/10.1002/2015JD023493, 2015.

Kuebbeler, M., Lohmann, U., and Feichter, J.: Effects of stratospheric sulfate aerosol geo-engineering on cirrus clouds, Geophysical Research Letters, 39, https://doi.org/10.1029/2012GL053797, l23803, 2012.

Kuhn, U. and Kesselmeier, J.: Environmental variables controlling the uptake of carbonyl sulfide by lichens, Journal of Geophysical Research: Atmospheres, 105, 26 783–26 792, https://doi.org/https://doi.org/10.1029/2000JD900436, 2000.

Laakso, A., Kokkola, H., Partanen, A.-I., Niemeier, U., Timmreck, C., Lehtinen, K. E. J., Hakkarainen, H., and Korhonen, H.: Radiative
and climate impacts of a large volcanic eruption during stratospheric sulfur geoengineering, Atmospheric Chemistry and Physics, 16,
305–323, https://doi.org/10.5194/acp-16-305-2016, 2016.

Labitzke, K. and McCormick, M. P.: Stratospheric temperature increases due to Pinatubo aerosols, Geophysical Research Letters, 19, 207–
210, https://doi.org/10.1029/91GL02940, 1992.

Lacis, A., Hansen, J., and Sato, M.: Climate forcing by stratospheric aerosols, Geophysical Research Letters, 19, 1607–1610,
https://doi.org/https://doi.org/10.1029/92GL01620, 1992.

Lamarque, J.-F., Dentener, F., McConnell, J., Ro, C.-U., Shaw, M., Vet, R., Bergmann, D., Cameron-Smith, P., Dalsoren, S., Doherty, R.,
Faluvegi, G., Ghan, S. J., Josse, B., Lee, Y. H., MacKenzie, I. A., Plummer, D., Shindell, D. T., Skeie, R. B., Stevenson, D. S., Strode, S.,
Zeng, G., Curran, M., Dahl-Jensen, D., Das, S., Fritzsche, D., and Nolan, M.: Multi-model mean nitrogen and sulfur deposition from the
Atmospheric Chemistry and Climate Model Intercomparison Project (ACCMIP): evaluation of historical and projected future changes,
Atmospheric Chemistry and Physics, 13, 7997–8018, https://doi.org/10.5194/acp-13-7997-2013, 2013.

Lee, C.-L. and Brimblecombe, P.: Anthropogenic contributions to global carbonyl sulfide, carbon disulfide and organosulfides fluxes, Earth-
Science Reviews, 160, 1–18, https://doi.org/https://doi.org/10.1016/j.earscirev.2016.06.005, 2016.

Lockley, A., MacMartin, D., and Hunt, H.: An update on engineering issues concerning stratospheric aerosol injection for geoengineering,
Environmental Research Communications, 2, 082 001, 2020.

MacMartin, D. G., Kravitz, B., Mills, M. J., Tribbia, J. J., Tilmes, S., Richter, J. H., Vitt, F., and Lamarque, J.-F.: The Climate Response
to Stratospheric Aerosol Geoengineering Can Be Tailored Using Multiple Injection Locations, Journal of Geophysical Research: Atmo-
spheres, 122, 12,574–12,590, https://doi.org/10.1002/2017jd026868, 2017.

Madon, H. N. and Strickland-Constable, R. F.: Production of CS2, Industrial & Engineering Chemistry, 50, 1189–1192, 1958.

Madronich, S., Tilmes, S., Kravitz, B., MacMartin, D. G., and Richter, J. H.: Response of surface ultraviolet and visible radiation to strato-
spheric SO2 injections, Atmosphere, 9, https://doi.org/10.3390/atmos9110432, 2018.

Meinshausen, M., Smith, S. J., Calvin, K., Daniel, J. S., Kainuma, M. L. T., Lamarque, J.-F., Matsumoto, K., Montzka, S. A., Raper, S. C. B.,
Riahi, K., Thomson, A., Velders, G. J. M., and van Vuuren, D. P. P.: The RCP greenhouse gas concentrations and their extensions from
1765 to 2300, Climatic Change, 109, 213, 2011.

Morgenstern, O., Giorgetta, M. A., Shibata, K., Eyring, V., Waugh, D. W., Shepherd, T. G., Akiyoshi, H., Austin, J., Baumgaertner, A.
J. G., Bekki, S., Braesicke, P., Brühl, C., Chipperfield, M. P., Cugnet, D., Dameris, M., Dhomse, S., Frith, S. M., Garny, H., Gettelman,
A., Hardiman, S. C., Hegglin, M. I., Jöckel, P., Kinnison, D. E., Lamarque, J.-F., Mancini, E., Manzini, E., Marchand, M., Michou, M.,
Nakamura, T., Nielsen, J. E., Olivié, D., Pitari, G., Plummer, D. A., Rozanov, E., Scinocca, J. F., Smale, D., Teyssèdre, H., Toohey,
M., Tian, W., and Yamashita, Y.: Review of the formulation of present-generation stratospheric chemistry-climate models and associated
external forcings, Journal of Geophysical Research, 115, D00M02, https://doi.org/10.1029/2009JD013728, 2010.

Morgenstern, O., Stone, K. A., Schofield, R., Akiyoshi, H., Yamashita, Y., Kinnison, D. E., Garcia, R. R., Sudo, K., Plummer, D. A.,
Scinocca, J., Oman, L. D., Manyin, M. E., Zeng, G., Rozanov, E., Stenke, A., Revell, L. E., Pitari, G., Mancini, E., Di Genova, G., Visioni,
D., Dhomse, S. S., and Chipperfield, M. P.: Ozone sensitivity to varying greenhouse gases and ozone-depleting substances in CCMI-1
simulations, Atmospheric Chemistry and Physics, 18, 1091–1114, https://doi.org/10.5194/acp-18-1091-2018, 2018.

Mu, Y., Geng, C., Wang, M., Wu, H., Zhang, X., and Jiang, G.: Photochemical production of carbonyl sulfide in precipitation, Journal of
Geophysical Research: Atmospheres, 109, https://doi.org/https://doi.org/10.1029/2003JD004206, 2004.

Neale, R. B., Richter, J., Park, S., Lauritzen, P. H., Vavrus, S. J., Rasch, P. J., and Zhang, M.: The Mean Climate of the Community Atmosphere Model (CAM4) in Forced SST and Fully Coupled Experiments, Journal of Climate, 26, 5150 – 5168, 2013.

Nowack, P. J., Abraham, N. L., Braesicke, P., and Pyle, J. A.: Stratospheric ozone changes under solar geoengineering: implications for UV exposure and air quality, Atmospheric Chemistry and Physics, 16, 4191–4203, https://doi.org/10.5194/acp-16-4191-2016, 2016.

Orbe, C., Yang, H., Waugh, D. W., Zeng, G., Morgenstern, O., Kinnison, D. E., Lamarque, J.-F., Tilmes, S., Plummer, D. A., Scinocca, J. F., Josse, B., Marecal, V., Jöckel, P., Oman, L. D., Strahan, S. E., Deushi, M., Tanaka, T. Y., Yoshida, K., Akiyoshi, H., Yamashita, Y., Stenke, A., Revell, L., Sukhodolov, T., Rozanov, E., Pitari, G., Visioni, D., Stone, K. A., Schofield, R., and Banerjee, A.: Large-scale tropospheric transport in the Chemistry–Climate Model Initiative (CCMI) simulations, Atmospheric Chemistry and Physics, 18, 7217–7235, 2018.

Pitari, G., Mancini, E., Rizi, V., and Shindell, D. T.: Impact of Future Climate and Emission Changes on Stratospheric Aerosols and Ozone, Journal of the Atmospheric Sciences, 59, 414–440, https://doi.org/10.1175/1520-0469(2002)059<0414:IOFCAE>2.0.CO;2, place: Boston MA, USA Publisher: American Meteorological Society, 2002.

Pitari, G., Aquila, V., Kravitz, B., Robock, A., Watanabe, S., Cionni, I., Luca, N. D., Genova, G. D., Mancini, E., and Tilmes, S.: Stratospheric ozone response to sulfate geoengineering: Results from the Geoengineering Model Intercomparison Project (GeoMIP), Journal of Geophysical Research: Atmospheres, 119, 2629–2653, https://doi.org/10.1002/2013JD020566, 2014.

Richter, J. H., Tilmes, S., Mills, M. J., Tribbia, J. J., Kravitz, B., Macmartin, D. G., Vitt, F., and Lamarque, J. F.: Stratospheric dynamical response and ozone feedbacks in the presence of SO2 injections, Journal of Geophysical Research: Atmospheres, 122, 12,557–12,573, https://doi.org/10.1002/2017JD026912, 2017.

Robock, A.: Volcanic eruptions and climate, Reviews of Geophysics, 38, 191–219, https://doi.org/10.1029/1998RG000054, 2000.

Roehl, C. M., Boglu, D., Brühl, C., and Moortgat, G. K.: Infrared band intensities and global warming potentials of CF4, C2F6, C3F8, C4F10, C5F12, and C6F14, Geophysical Research Letters, 22, 815–818, https://doi.org/https://doi.org/10.1029/95GL00488, 1995.

Sandoval-Soto, L., Stanimirov, M., von Hobe, M., Schmitt, V., Valdes, J., Wild, A., and Kesselmeier, J.: Global uptake of carbonyl sulfide (COS) by terrestrial vegetation: Estimates corrected by deposition velocities normalized to the uptake of carbon dioxide (CO_2), Biogeosciences, 2, 125–132, https://doi.org/10.5194/bg-2-125-2005, 2005.

Smith, C. J., Kramer, R. J., Myhre, G., Alterskjær, K., Collins, W., Sima, A., Boucher, O., Dufresne, J.-L., Nabat, P., Michou, M., Yukimoto, S., Cole, J., Paynter, D., Shiogama, H., O'Connor, F. M., Robertson, E., Wiltshire, A., Andrews, T., Hannay, C., Miller, R., Nazarenko, L., Kirkev\aag, A., Olivié, D., Fiedler, S., Lewinschal, A., Mackallah, C., Dix, M., Pincus, R., and Forster, P. M.: Effective radiative forcing and adjustments in CMIP6 models, Atmospheric Chemistry and Physics, 20, 9591–9618, https://doi.org/10.5194/acp-20-9591-2020, 2020.

Smith, W. and Wagner, G.: Stratospheric aerosol injection tactics and costs in the first 15 years of deployment, Environmental Research Letters, 13, 124 001, https://doi.org/10.1088/1748-9326/aae98d, 2018.

Steinbacher, M., Bingemer, H. G., and Schmidt, U.: Measurements of the exchange of carbonyl sulfide (OCS) and carbon disulfide (CS2) between soil and atmosphere in a spruce forest in central Germany, Atmospheric Environment, 38, 6043–6052, https://doi.org/https://doi.org/10.1016/j.atmosenv.2004.06.022, 2004.

Stimler, K., Montzka, S. A., Berry, J. A., Rudich, Y., and Yakir, D.: Relationships between carbonyl sulfide (COS) and CO2 during leaf gas exchange, New Phytologist, 186, 869–878, https://doi.org/https://doi.org/10.1111/j.1469-8137.2010.03218.x, 2010.

Svoronos, P. D. N. and Bruno, T. J.: Carbonyl Sulfide: A Review of Its Chemistry and Properties, Industrial & Engineering Chemistry Research, 41, 5321–5336, https://doi.org/https://doi.org/10.1021/ie020365n, 2002.

Tilmes, S., Müller, R., and Salawitch, R.: The Sensitivity of Polar Ozone Depletion to Proposed Geoengineering Schemes, Science, 320, 1201–1204, https://doi.org/10.1126/science.1153966, 2008.

Tilmes, S., Garcia, R. R., Kinnison, D. E., Gettelman, A., and Rasch, P. J.: Impact of geoengineered aerosols on the troposphere and strato-
sphere, Journal of Geophysical Research: Atmospheres, 114, https://doi.org/https://doi.org/10.1029/2008JD011420, 2009.

Tilmes, S., Mills, M. J., Niemeier, U., Schmidt, H., Robock, A., Kravitz, B., Lamarque, J.-F., Pitari, G., and English, J. M.: A new Geoengi-
neering Model Intercomparison Project (GeoMIP) experiment designed for climate and chemistry models, Geoscientific Model Develop-
ment, 8, 43–49, https://doi.org/10.5194/gmd-8-43-2015, 2015.

Tilmes, S., Richter, J. H., Kravitz, B., Macmartin, D. G., Mills, M. J., Simpson, I. R., Glanville, A. S., Fasullo, J. T., Phillips, A. S., Lamarque,
J. F., Tribbia, J., Edwards, J., Mickelson, S., and Ghosh, S.: CESM1(WACCM) stratospheric aerosol geoengineering large ensemble
project, Bulletin of the American Meteorological Society, pp. 2361–2371, https://doi.org/10.1175/BAMS-D-17-0267.1, 2018a.

Tilmes, S., Richter, J. H., Mills, M. J., Kravitz, B., MacMartin, D. G., Garcia, R. R., Kinnison, D. E., Lamarque, J. F., Tribbia, J., and Vitt, F.:
Effects of Different Stratospheric SO2 Injection Altitudes on Stratospheric Chemistry and Dynamics, Journal of Geophysical Research:
Atmospheres, 123, 4654–4673, https://doi.org/10.1002/2017JD028146, 2018b.

Tilmes, S., Richter, J. H., MacMartin, D. G., Kravitz, B., Glanville, A., Visioni, D., , Kinnison, D., and Mueller, R.: Sensitivity of total
column ozone to stratospheric sulfur injection strategies, Geophysical Research Letters, n/a, n/a, inreview, 2021.

Trisos, C. H., Amatulli, G., Gurevitch, J., Robock, A., Xia, L., and Zambri, B.: Potentially dangerous consequences for biodiversity of solar
geoengineering implementation and termination, Nature Ecology & Evolution, 2, 475–482, https://doi.org/10.1038/s41559-017-0431-0,
2018.

Ulshofer, V., Flock, O., Uher, G., and Andreae, M.: Photochemical production and air-sea exchange of carbonyl sulfide in the eastern
Mediterranean Sea, Marine Chemistry, 53, 25–39, 1996.

Van Diest, H. and Kesselmeier, J.: Soil atmosphere exchange of carbonyl sulfide (COS) regulated by diffusivity depending on water-filled
pore space, Biogeosciences, 5, 475–483, https://doi.org/10.5194/bg-5-475-2008, 2008.

Vattioni, S., Weisenstein, D., Keith, D., Feinberg, A., Peter, T., and Stenke, A.: Exploring accumulation-mode H2SO4 versus SO2 strato-
spheric sulfate geoengineering in a sectional aerosol-chemistry-climate model, Atmospheric Chemistry and Physics, 19, 4877–4897,
https://doi.org/10.5194/acp-19-4877-2019, 2019.

Visioni, D., Pitari, G., Aquila, V., Tilmes, S., Cionni, I., Di Genova, G., and Mancini, E.: Sulfate geoengineering impact on methane transport
and lifetime: results from the Geoengineering Model Intercomparison Project (GeoMIP), Atmospheric Chemistry and Physics, 17, 11 209–
11 226, https://doi.org/10.5194/acp-17-11209-2017, 2017a.

Visioni, D., Pitari, G., Aquila, V., Tilmes, S., Cionni, I., Di Genova, G., and Mancini, E.: Sulfate geoengineering impact on methane transport
and lifetime: results from the Geoengineering Model Intercomparison Project (GeoMIP), Atmospheric Chemistry and Physics, 17, 11 209–
11 226, https://doi.org/10.5194/acp-17-11209-2017, 2017b.

Visioni, D., Pitari, G., Di Genova, G., Tilmes, S., and Cionni, I.: Upper tropospheric ice sensitivity to sulfate geoengineering, Atmospheric
Chemistry and Physics, https://doi.org/10.5194/acp-18-14867-2018, 2018a.

Visioni, D., Pitari, G., Tuccella, P., and Curci, G.: Sulfur deposition changes under sulfate geoengineering conditions: Quasi-biennial oscil-
lation effects on the transport and lifetime of stratospheric aerosols, Atmospheric Chemistry and Physics, https://doi.org/10.5194/acp-18-
2787-2018, 2018b.

Visioni, D., Pitari, G., Tuccella, P., and Curci, G.: Sulfur deposition changes under sulfate geoengineering conditions: quasi-biennial
oscillation effects on the transport and lifetime of stratospheric aerosols, Atmospheric Chemistry and Physics, 18, 2787–2808,
https://doi.org/10.5194/acp-18-2787-2018, 2018c.

Visioni, D., MacMartin, D. G., Kravitz, B., Tilmes, S., Mills, M. J., Richter, J. H., and Boudreau, M. P.: Seasonal Injection Strategies for Stratospheric Aerosol Geoengineering, Geophysical Research Letters, 46, 7790–7799, https://doi.org/10.1029/2019GL083680, 2019.

Visioni, D., MacMartin, D. G., Kravitz, B., Lee, W., Simpson, I. R., and Richter, J. H.: Reduced Poleward Transport Due to Stratospheric Heating Under Stratospheric Aerosols Geoengineering, Geophysical Research Letters, 47, e2020GL089 470, https://doi.org/https://doi.org/10.1029/2020GL089470, e2020GL089470 10.1029/2020GL089470, 2020.

Visioni, D., MacMartin, D. G., and Kravitz, B.: Is Turning Down the Sun a Good Proxy for Stratospheric Sulfate Geoengineering?, Journal of Geophysical Research: Atmospheres, 126, e2020JD033 952, https://doi.org/https://doi.org/10.1029/2020JD033952, e2020JD033952 2020JD033952, 2021a.

Visioni, D., MacMartin, D. G., Kravitz, B., Boucher, O., Jones, A., Lurton, T., Martine, M., Mills, M. J., Nabat, P., Niemeier, U., Séférian, R., and Tilmes, S.: Identifying the sources of uncertainty in climate model simulations of solar radiation modification with the G6sulfur and G6solar Geoengineering Model Intercomparison Project (GeoMIP) simulations, Atmospheric Chemistry and Physics, 21, 10 039–10 063, https://doi.org/10.5194/acp-21-10039-2021, 2021b.

Wang, L., Yang, Y., Shen, W., Kong, X., Li, P., Yu, J., and Rodrigues, A. E.: CO2 Capture from Flue Gas in an Existing Coal-Fired Power Plant by Two Successive Pilot-Scale VPSA Units, Industrial & Engineering Chemistry Research, 52, 7947–7955, 2013.

West, J. J. and Fiore, A. M.: Management of Tropospheric Ozone by Reducing Methane Emissions, Environmental Science & Technology, 39, 4685–4691, https://doi.org/10.1021/es048629f, pMID: 16053064, 2005.

Whelan, M. E., Hilton, T. W., Berry, J. A., Berkelhammer, M., Desai, A. R., and Campbell, J. E.: Carbonyl sulfide exchange in soils for better estimates of ecosystem carbon uptake, Atmospheric Chemistry and Physics, 16, 3711–3726, 2016.

Xia, L., Nowack, P. J., Tilmes, S., and Robock, A.: Impacts of stratospheric sulfate geoengineering on tropospheric ozone, Atmospheric Chemistry and Physics, 17, 11 913–11 928, https://doi.org/10.5194/acp-17-11913-2017, 2017a.

Xia, L., Nowack, P. J., Tilmes, S., and Robock, A.: Impacts of stratospheric sulfate geoengineering on tropospheric ozone, Atmospheric Chemistry and Physics, 17, 11 913–11 928, https://doi.org/10.5194/acp-17-11913-2017, 2017b.